Nanoscale

PAPER

View Article Online
View Journal | View Issue

Check for updates

Cite this: *Nanoscale*, 2020, **12**, 18864

A nanostructured anti-biofilm surface widens the efficacy against spindle-shaped and chain-forming rod-like bacteria†

Xin Li,‡[a,b] Kwong-Hoi Tsui,‡[c,d] James K. H. Tsoi,[d] David W. Green,[e] Xiao-zhuang Jin,[d] Yong Qiang Deng,[b] Yao Min Zhu,[b] Xu Guang Li,[b] Zhiyong Fan *[c] and Gary Shun-pan Cheung *[a]

Current control of pathogenic bacteria at all biomaterial interfaces is poorly attuned to a broad range of disease-causing pathogens. Leading antimicrobial surface functionalization strategies with antimicrobial peptides (AMPs), defensins, have not shown their promised efficacy. One of the main problems is the lack of stability and swift clearance from the surface. Surface nanotopography bearing sharp protrusions is a non-chemical solution that is intrinsically stable and long-lasting. Previously, the geometrically ordered arrays of nanotipped spines repelled or rapidly ruptured bacteria that come into contact. The killing properties so far work on cocci and rod-like bacteria, but there is no validation of the efficacy of protrusional surfaces on pathogenic bacteria with different sizes and morphologies, thus broadening the utility of such surfaces to cover increasingly more disease entities. Here, we report a synthetic analogue of nanotipped spines with a pyramidal shape that show great effectiveness on species of bacteria with strongly contrasting shapes and sizes. To highlight this phenomenon in the field of dental applications where selective bacterial control is vital to the clinical success of biomaterial functions, we modified the poly(methyl)-methacrylate (PMMA) texture and tested it against *Streptococcus mutans*, *Enterococcus faecalis*, *Porphyromonas gingivalis*, and *Fusobacterium nucleatum*. These nanopyramids performed effectively at levels well above those of normal and roughened PMMA biomaterials for dentistry and a model material for general use in medicine and disease transmission in hospital environments.

Received 16th May 2020,
Accepted 2nd August 2020

DOI: 10.1039/d0nr03809a

rsc.li/nanoscale

Published on 05 August 2020. Downloaded on 4/22/2021 7:05:35 AM.

1. Introduction

Biofilms are an immobilized community of microorganisms with a propensity to adhere to an extensive range of natural, inanimate, and synthetic surfaces.[1] The biofilm population comprises a kaleidoscopic consortium of bacteria, fungi, and amoeba, which cross-feed one another. Medical biofilms are the leading cause of 10% of all hospital-based infections and the leading cause of implant failures worldwide. In the USA, 100 000 people die from persistent biofilm infections. Estimates put 80% of total chronic microbial infections as a biofilm.[2]

In the human body, the biofilm antagonizes the host's immunity into lengthening persistence and virulence. Examples of antagonism as an evolved strategy include the inflammatory reactions of gingiva and periodontium to the accumulation of dental plaque, a unique type of biofilm that is adherent to the root surface of teeth;[3] denture-induced stomatitis to the accumulation of a microbial biofilm on the material surface;[4] and ocular infection from the buildup of a biofilm on contact lenses and intraocular lens.[5] Artificial medical devices, sutures, and catheters, routinely used in surgery and hospitals, respectively, are highly susceptible to microbial contamination, population, and biofilm formation.[6] Polymeric biomaterials are particularly featured.

Poly(methyl)-methacrylate, or PMMA, is in widespread use in many medical and dental appliances.[7] Given the water sorption ability and surface irregularities after fabrication, bacteria can readily colonize on the surface of PMMA.[4] The material itself may become weakened.[8] The oral cavity is the most

[a]*Division of Restorative Dental Sciences, Faculty of Dentistry, PPDH 34 Hospital Road, The University of Hong Kong, Pokfulam, Hong Kong SAR, China. E-mail: spcheung@hku.hk*
[b]*Department of Stomatology, Shenzhen University General Hospital, Shenzhen University Clinical Medical Academy, 1098 Xuan Yuan Road, Nanshan District, Shenzhen, Guangdong Province, 518055 China*
[c]*Department of Electronic and Computer Engineering, Hong Kong University of Science and Technology, Clear Water Bay, Kowloon, Hong Kong SAR, China*
[d]*Applied Oral Sciences, Faculty of Dentistry, PPDH 34 Hospital Road, The University of Hong Kong, Pokfulam, Hong Kong SAR, China*
[e]*IPME, College of Biomedical Engineering, Taipei Medical University, 250 Wu-Xing Street, Taipei 11031, Taiwan*

†Electronic supplementary information (ESI) available. See DOI: 10.1039/d0nr03809a

‡These authors contributed equally to this work as first authors.

This journal is © The Royal Society of Chemistry 2020

Published on 05 August 2020. Downloaded on 4/22/2021 7:05:35 AM.

microbially polluted environment in the human body, such that more than 600 different species of bacteria and over 100 million bacterial cells may be recovered in every milliliter of saliva.[9] A fraction of this number is potential pathogens or existing ones. Once biofilms establish themselves as an adherent coating on the surface, they are exceedingly difficult to remove by any chemical and physical means.

For instance, biofilms exposed to chlorine for 60 minutes can still contain living cells, and individual cells within a biofilm can persist in an iodine solution for up to 15 minutes.[10] Antibiotics are becoming increasingly less effective, as many bacteria have developed antibiotic resistance.[11] In addition, the desired or functional properties of the materials may be negatively affected.[12] Some chemicals might not be biocompatible or, even, exhibit toxicity, *i.e.*, not safe for use on humans,[13,14] and hence should not be used as additives in PMMA. Physical disruption of the bacterial biofilm may work on the PMMA surface but only to varying degrees.[15]

Modifying the surfaces of medical biomaterials in specific forms at the microscale and nanoscale effectively reduces microbial accumulation.[16] Surface modification interferes, in some cases, with one part in the sequence of biofilm formation, and due to its experimental success, it is now a popular strategy.[17] Surface modification is the cosmetic augmentation of a material and does not affect the bulk properties. Since cells respond acutely to nanoscale features,[18] there are approaches harnessing the surface nanostructures to control the microbial attachment and growth. These small structures range among nanoprotrusions (spikes and spines), nanopillars, nanomounds, and nanovalleys. The interplay between nanostructures and microbes determines the attachment probabilities, the strength of adherence and organisation as well as the possibilities for colonization.[18]

The size, shape, and pattern of the surface nanostructure are the factors that might alter its antibacterial efficacy.[19,20] Surface protrusions with high aspect ratios, sharp edges, and tight packing are in focus. Biophysical approaches to control bacteria are promising, because there is low probability of emerging adaptations defying the laws of physics.[20–23] The trade-offs involved in developing a cell wall with equivalent stiffness to that of the material are highly unresolvable.

Theoretically, bacteria-repellent surfaces can prevent biofilm formation and biofilm-mediated diseases without the need for any chemical agents already with provable efficaciousness and a longstanding track record of killing microorganisms. In contrast to physical processes of killing, bacteria can adapt to toxic chemicals over many generations. Two main biophysical mechanisms are at play between the surface protrusions and colonising bacteria: the repellent formations and the bactericidal formations.

The former refers to the bacteria-repellent properties of a surface to prevent the buildup or accumulation of biological materials.[24] For the second mechanism, the surface nanostructures may allow the attachment to bacteria; however, they exhibit a bactericidal action, destroying the adherent microbial cells. Some authors referred them as biocidal surfaces.[21,23] While the eventual manifestation of either action is a significantly reduced accumulation of microorganisms, thus preventing biofilm-mediated diseases without the need for any chemical agents, the underpinning mechanisms are different. Some surfaces might exhibit both actions, although the relative contribution of each action may differ.

Pathogenic bacteria are attracted to biomaterials from various sources. They may arrive externally or arise internally when the population ecology changes. This study is concerned with a model biomaterial exposed to dental pathogens, to prove the effectiveness of pyramid arrays. *Streptococcus mutans*, a Gram-positive facultative anaerobe, is one of the first colonizers adhering to the tooth surface and is a significant contributor to dental decay. *Enterococcus faecalis* is a close cousin of *S. mutans* and is present in healthy individuals. It is an opportunistic organism that is triggered into pathogenesis by an ecological change in the population. It is prevalent after root canal treatment (70–90% of failed cases) and dental implantation. *Porphyromonas gingivalis* is a short rod, Gram-negative, obligatory anaerobe that is the primary pathogen for gum and periodontal diseases. Finally, *Fusobacterium nucleatum* is another turncoat oral bacterium that is involved in gum disease, and an important intermediate colonizer that facilitates the coaggregation of other bacteria in the development of biofilms.[25] Tooth decay and gum disease are two of the most prevalent non-communicable diseases affecting humans.[26] These examples broadly represented the pathogenic portfolio in the oral cavity with tremendous clinical significance.

The biophysical mechanism for killing adherent bacteria mediates through the surface features of nanoscale dimensions. For example, the cicada wing has a nanopatterned array of 200 nm-high pillars spaced 170 nm apart, which is potently biocidal against *Pseudomonas aeruginosa*, by mechanically penetrating through the cell wall and membrane within several minutes after the bacterial adhesion process begins.[21,24] Another example is the gecko skin that shows similar biophysical antimicrobial action.[27] Replicas of the gecko skin in a polymeric material also possess bactericidal effects against *S. mutans*,[28] *P. gingivalis*, and *Escherichia coli.*[29] Many studies of the biocidal properties of the nanopatterned surface have used only one bacterial species for the demonstration of the effect. Testing with a broader selection of clinically relevant bacterial species should provide more meaningful results. Besides, more data are needed to connect the individual design elements among the range of possible designs with their effects on bacteria. Of particular relevance to bacterial destruction by tearing, repelling, and rupturing[30] is the presence of nanospikes, aspect ratio of the protrusions and spacings between the protrusions.[20] These high aspect nanoprotuberances apply to bacterial killing, repelling with relevance to fungal spore destruction, and the possibility of disrupting the lipid envelope of certain large viruses. Self-cleaning occurs on nano-protrusion surfaces and this process can be harnessed to clear proteins and other contaminant particles from those surfaces.[31] The surface protrusions also have positive and negative effects on human cells (depending on cell

Published on 05 August 2020. Downloaded on 4/22/2021 7:05:35 AM.

type), so that they can be applied to tissue engineering strategies.[19,32] One application is a surface coating to enhance and strengthen tissue adhesion.[31] In this study, we employed a novel photolithography-based approach to fabricate biomimetic nanostructured surfaces in a PMMA material and exposed to an aqueous environment laden with three contrasting types of bacteria: round, rod-shaped, and spindle-shaped. Specifically, this study aimed to determine the antibacterial and bactericidal effects of synthetic surface nano-protuberances with three separate heights, widths, and aspect ratios. These were tested against several oral bacterial morphotypes bearing slightly varying shapes, cell wall ultra-structures, wall thicknesses, and interactomes. The study serves as a testbed for adapting techniques that can accurately specify the protrusion dimensionality in a polymer and function against several bacteria for a niche application.

2. Materials and methods

2.1 Fabrication of PMMA films with surface nanopatterns of different aspect ratios

A technique using the principle of photolithography and wet etching was used to produce a mold for casting with PMMA (Fig. 1). Briefly, a clean (111)-oriented silicon (Si) wafer with a 100 nm-thick surface oxide layer was coated with a photoresist, which was patterned with photolithography to obtain a regular array of square holes with a pitch of 1.5 μm (Fig. 1a). Then, the patterned surface was etched with benzoxazolinone (BOA) to remove the exposed silicon oxide layer, producing a regular array of nanoscale inversed pyramids in the Si wafer. The etching time would control the size of the inversed pyramids; etching for 50 min produced the most closely packed pyramids. After removing the photoresist, the wafer was then placed in 15% tetramethylammonium hydroxide (TMAH) solution at 50 °C for 50 min for wet etching (Fig. 1b). Thereafter, different thicknesses (400 nm, 800 nm and 1200 nm) of chromium (Cr) was sputtered on the Si wafer to form the mold (Fig. 1c). The amount of sputter coating deposited would determine the aspect ratio of the surface nanopyramids after casting. For the casting process, the PMMA solution was prepared by dissolving 10 g of PMMA powder (Alfa Aesar; Thermo Fisher Scientific, Heysham, UK) in 100 mL of toluene (Analytical grade, RCI Labscan, Bangkok, Thailand), and the solution was poured on the surface of the Cr-coated Si wafer and heat cured at 90 °C for 1 h and then at 120 °C for another 30 min. A transparent PMMA film with nanopyramids on the surface was obtained after peeling off from the mold (Fig. 1d). Cr appeared to also serve as an anti-sticking layer such that the mold could be used multiple times without leaving any residues. Four groups of the PMMA specimen were prepared for characterization: (1) NP400 (from a mold sputter coated with 400 nm Cr); (2) NP800 (with 800 nm Cr); (3) NP1200 (with 1200 nm Cr); (4) non-textured, *i.e.* smooth, flat PMMA (the control group).

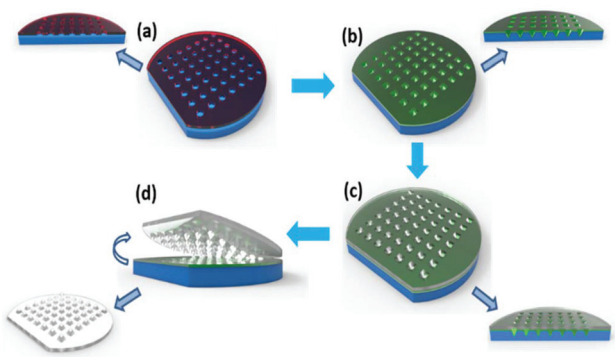

Fig. 1 Schematics of nanopyramidal PMMA film fabrication: (a) A ⟨100⟩ oriented Si wafer with a 100 nm SiO_2 surface that had undergone photolithography with a 1.5 μm square array pattern and BOA etching; (b) the patterned wafer having undergone TMAH wet etching to form an inverted-pyramid template; (c) different thicknesses of Cr sputtered on the surface; and (d) a regular nanopyramid on the PMMA film after peeling off.

2.2 Characterizations

The arithmetic average values of the roughness profile (R_a) were obtained using an AFM (dimension edge with ScanAsyst™; Bruker, Santa Barbara, CA, USA), and the calculations for surface roughness and micro-hardness were carried out using the supplied software (NanoScope Analysis 1.5; Bruker, Santa Barbara). Furthermore, the static water contact angle (WCA) value was measured using a contact angle goniometer (SL200KB; KINO, Norcross, GA, USA) with the surface free energy (SFE) estimated using the software (CAST3.0; KINO, Norcross). All specimens were then affixed on copper holders, sputter-coated with gold using a magnetron sputtering deposition system (Dynavac CS300, Hingham, MA, USA) for 100 s, and examined using a field-emission scanning electron microscope (JSM-7800F; JOEL, Peabody, MA, USA) operating at 5 kV. The high-resolution micrographs of the surface topographies were obtained at different magnifications (×5000, ×10 000 and ×20 000).

2.3 Biofilm cultivation and examination

Four representative pathogenic bacteria were selected for use in this study: *S. mutans* (ATCC 33277; American Type Culture Collection, Manassas, VA, USA); *E. faecalis* (ATCC 29212); *P. gingivalis* (ATCC 35668); *F. nucleatum* (ATCC 25586). *E. faecalis* and *F. nucleatum* were frequently isolated from root canal failures, whereas *S. mutans* and *P. gingivalis* from the tooth and root surfaces, respectively. Prior to the experiment, each species of bacteria was inoculated on a blood agar plate and cultured anaerobically for 24 h. Then, a scoop of bacteria was taken from one colony and transferred into a sterile broth for preparing a bacterial suspension. *S. mutans* and *E. faecalis* were added to a brain heart infusion (BHI) broth (Oxoid™, Thermo Fisher Scientific, Basingstoke, Hampshire, UK), whereas *P. gingivalis* and *F. nucleatum* were cultured in a broth containing (in 1 L) 30 g of tryptic soy broth (TSB) (Difco; Becton Dickinson, Franklin Lakes, NJ, USA), 5 g of yeast extract

 This journal is © The Royal Society of Chemistry 2020

Published on 05 August 2020. Downloaded on 4/22/2021 7:05:35 AM.

(Difco) and 10 mL of hemin (Sigma-Aldrich; St Louis, MO, USA). The suspensions were titrated to OD660 = 0.500–0.517 with a spectrophotometer (DU® 730 Life Science UV/vis Spectrophotometer; Beckman Coulter, Brea, CA, USA), which corresponds to a concentration of 1.0×10^9 CFU mL^{-1} (McFarland standard 4). Segments of the PMMA films (size 0.5 cm × 0.5 cm, $n = 3$ for each group) were sterilized with 4% Clorox before use for 10 min, and rinsed with sterilized distilled water for 1 min. The PMMA samples were placed, with the nanopatterned surface facing upward to allow bacterial adhesion, inside individual culture wells of a sterile 24-well culture plate (Corning Glass Works, New York, USA), into which 1 mL of the bacterial suspension was added. The aseptic technique was strictly followed. All samples were then incubated anaerobically (atmosphere $N_2 : CO_2 : H_2 = 8 : 1 : 1$ by volume) at 37 °C for 1 h, 24 h, 72 h or 168 h, before microscopic examinations. The broth was replaced daily during the incubation period.

2.4 Microscopy examinations

Two microscopy methods were employed to examine the bacterial vitality, distribution, morphology, and adhesion, and subsequently calculate and determine the killing/impairing efficiency for each surface. First, each specimen was stained using a LIVE/DEAD BacLight™ Bacterial Viability Kit (L7012 Invitrogen; Molecular Probes, Eugene, OR, USA) in the dark at room temperature for 30 min. The growth of bacteria was calculated for each specimen from the green and red fluorescence signals (representing live and dead bacterial cells, respectively) using a confocal laser scanning microscope (CLSM) (IX81 FluoView FV1000; Olympus, Shinjuku-ku, Tokyo, Japan). Six independent and randomly selected areas were imaged from each specimen. All CLSM images were imported into the computer, and the amount of live and dead bacterial cells in every observation field was determined using an image analysis software (ImageJ; National Institutes of Health, Bethesda, Maryland, USA). All quantitative data were analysed with statistical software (SPSS 11.0; SPSS Inc., Chicago, IL, USA).

After CLSM examination, the specimens were retrieved and fixed in 2.5% glutaraldehyde solution for 1 h. Then, they were serially dehydrated by increasing the concentrations of ethanol, from 70% up to 100%. The samples were then inspected using a field-emission scanning electron microscope (JSM-7800F) operating at 5 kV. The high-resolution micrographs of the nanopattern and the morphological appearance of the bacterial cells on each surface were recorded at different magnifications (×5000, ×10 000, and ×20 000).

3. Results

3.1 Characterization of the nanopatterned surface

Nanoscale pyramidal protrusions on the PMMA surface were observed in all groups (Fig. 2). Group NP400 showed low-rise, square based nanoscale pyramids with an aspect ratio of 1 (Fig. 2a). The spinules/nanospikes in group NP800 were taller,

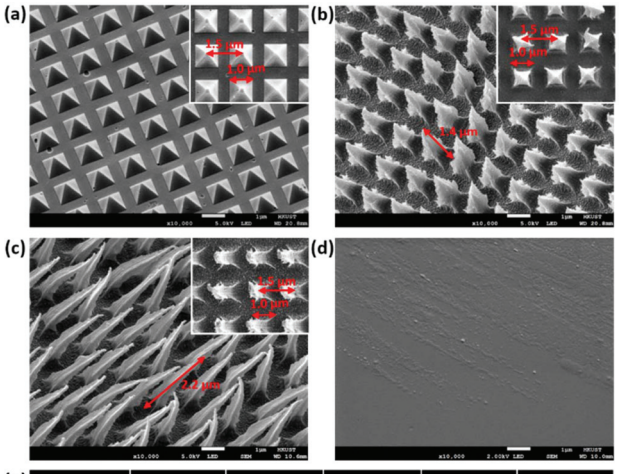

Group	Periodicity (μm)	Spacing (nm)	Height (μm)	Width (μm)	Aspect ratio
NP400	1.5	500	1.0	1.0	1.0
NP800	1.5	500	1.4	1.0	1.4
NP1200	1.5	500	2.2	1.0	2.2

Fig. 2 SEM micrographs showing the topographies of different nanopatterned PMMA surfaces: (a) NP400, (b) NP800, (c) NP1200, and (d) smooth control; and (e) the measured parameters of the surface PMMA nano- features (scale bar = 1 μm, magnification: ×10 000).

at about 2 μm, with an aspect ratio of about 1.4 and with a more definite pointed tip (Fig. 2b). The NP1200 group showed slender spinules of about 3 μm tall, with pointed tips and an aspect ratio greater than 2 (Fig. 2c). Some variations in the spinule height of groups NP800 and NP1200 were noted. The periodicity, or the distance between the centers of the nanopyramidal base of each spinule, was measured to be 1.5 μm – the distance being the same as was specified for the photolithographic equipment. By deduction, the distance between the base of each nanopyramid and its neighbors was 500 nanometers.

The R_a value of the nanopatterned surfaces was 43.7 ± 2.65 nm for NP400, 53.1 ± 8.78 nm (for NP800), and 108.0 ± 13.4 nm for the NP1200 group. All of them were statistically different from those of the smooth control (15.9 ± 2.9 nm) ($p < 0.05$). The static WCA values increased significantly from 78.68° (control) to about 90° for NP400, or greater (111.27 ± 0.16° for NP800; 93.63 ± 0.20° for NP1200) – the corresponding SFE values of all nanopatterned surfaces tested were significantly lower than that of the control group (Table 1). The NP800 group was noted to have the greatest contact angle, with the lowest free surface energy.

3.2 Bacterial viability and adhesion

3.2.1 ***Streptococcus mutans*.** CLSM examination showed a significant reduction in the amounts of live *S. mutans* cells, but an increase in dead ones, either in absolute amount or in terms of proportion, at various time points throughout the incubation period, when compared to the control group (Fig. 3 and ESI Fig. 1†).

Published on 05 August 2020. Downloaded on 4/22/2021 7:05:35 AM.

Table 1 Static water contact angle (WCA) and calculated surface free energy (SFE) for each group

Group	WCA (°)	SFE (J m^{-2})	Drop profile
Control	78.68 ± 0.00	35.20 ± 0.04	
NP400	88.59 ± 0.20	29.08 ± 0.12	
NP800	111.27 ± 0.16	15.62 ± 0.09	
NP1200	93.63 ± 0.20	26.00 ± 0.12	

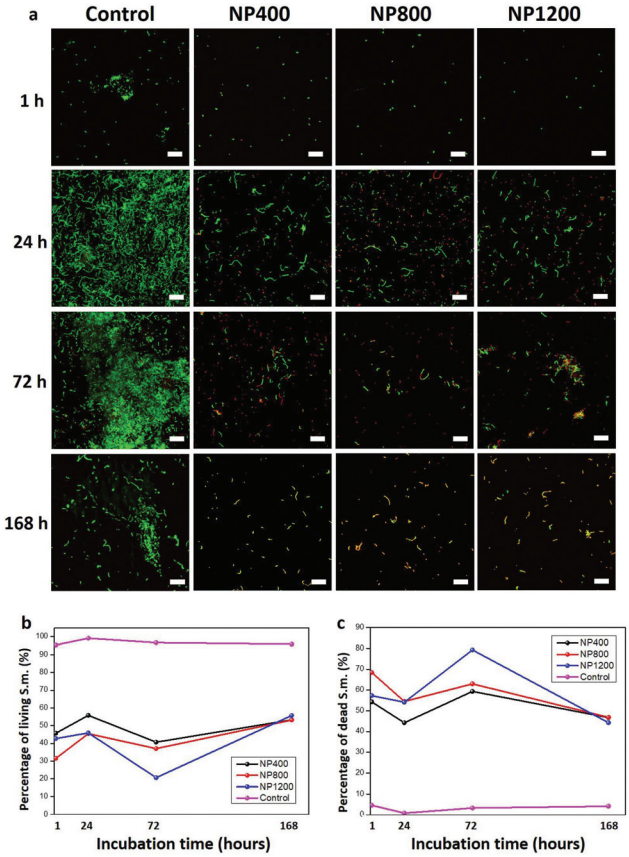

Fig. 3 Viability of *S. mutans* on different surfaces at different incubation times: (a) CLSM images of live (green) and dead (red) bacterial cells; (b) percentage of live *S. mutans*; and (c) percentage of dead *S. mutans* (measurement area = 126 × 126 μm^2 and image size = 640 × 640 pixels) (error bars = 95% CI, *p < 0.05).

The SEM appearance of the bacterial aggregates of the control group was in stark contrast to those on the nano-patterned surfaces (Fig. 4). The bacterial cells gathered on the smooth PMMA surface of the control group, which became denser and thicker at longer incubation periods. The outline of individual cells could be identified. In contrast, *S. mutans* failed to congregate into any form of organized mass in all

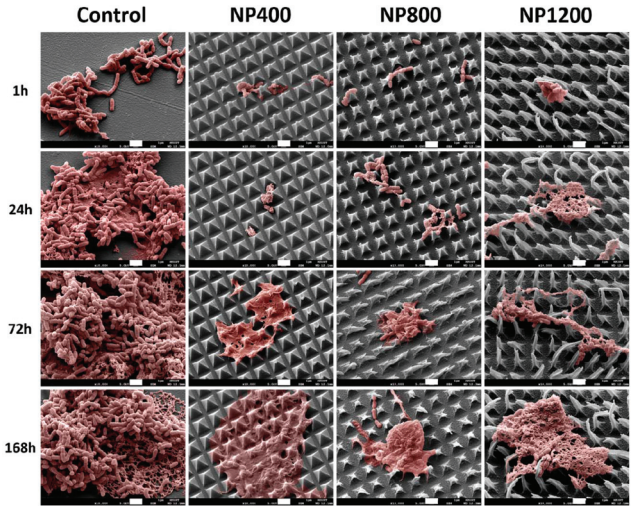

Fig. 4 SEM images of *S. mutans* (colored in pink in the image manipulation software (Photoshop CS6; Adobe, USA)) on different PMMA surfaces after different periods of incubation (scale bar = 1 μm, magnification: ×10 000).

experimental groups. Instead, the bacterial cells were found only in very small clusters. After 1 day of incubation, all experimental groups with a nano-patterned surface, despite the different aspect ratios of their nanostructure, showed an apparently high degree of biofilm repellency, with the bacterial cells remaining isolated or only gathering in tiny aggregates. Where clusters of *S. mutans* were found, they often were situated in between, and some near the pointed tips of the nanospinules. The appearance was similar after 3 days to 1 week of incubation – the nano-patterned surfaces remained with little sign of biofilm formation or with the biofilm being severely disrupted. For those (small) areas with the accumulation of *S. mutans*, the colonies looked very different from that of the control group and they appeared very thin, with the outline of individual cells being either blur or unidentifiable. The nanospinules of the NP1200 groups appeared flexible.

3.2.2 *Enterococcus faecalis*. For the experimental nano-patterned groups, *E. faecalis* demonstrated a very similar trend of a significant reduction in live bacterial cells, but an increase in dead ones, at various time points throughout the incubation period (Fig. 5 and ESI Fig. 2†). The proportion of live cells dropped to an apparent minimum after 3 days, and gradually increased in number at 1 week, although the total amount of bacteria remained significantly lower than the control.

Similar to the observations for *S. mutans*, there were stark differences in the colonization of *E. faecalis* on the nanopatterned surfaces *versus* the smooth PMMA surface (Fig. 6). At 1 hour post-incubation, some isolated bacterial cells were either "trapped" in between the nanospinules, or situated at or close to the tips, while the bacterial cells were clustered on the smooth control surface. After 1 day of incubation, thick aggregates of *E. faecalis* cells and some extracellular materials were present, covering a large part of the smooth surface; a similar

This journal is © The Royal Society of Chemistry 2020

Published on 05 August 2020. Downloaded on 4/22/2021 7:05:35 AM.

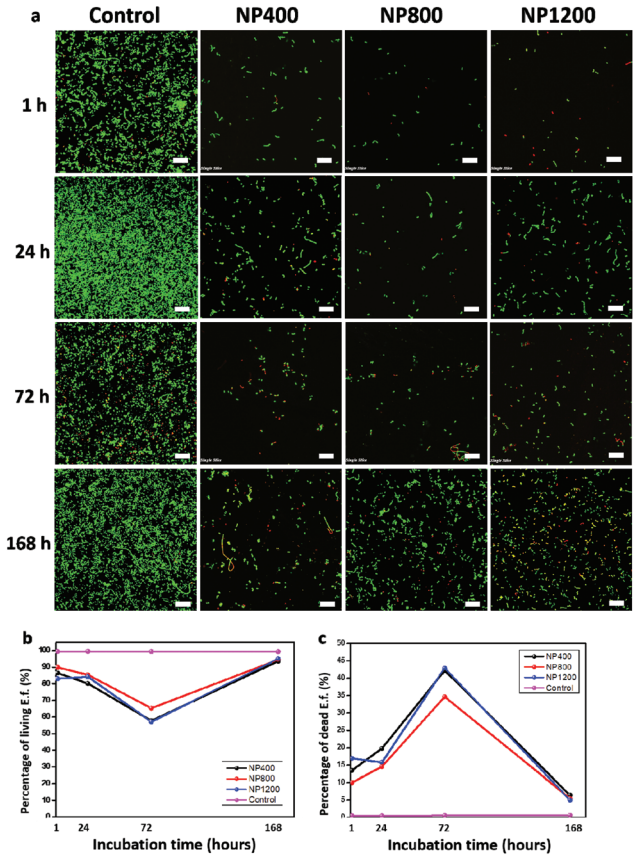

Fig. 5 Viability of *E. faecalis* on different surfaces at different incubation times: (a) CLSM images of live (green) and dead (red) bacterial cells; (b) percentage of live *E. faecalis*; and (c) percentage of dead *E. faecalis* (measurement area = 126 × 126 μm^2 and image size = 640 × 640 pixels) (error bars = 95% CI, *p < 0.05).

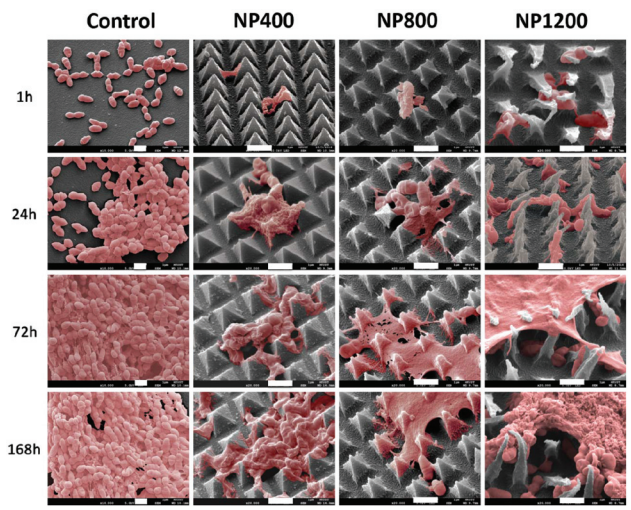

Fig. 6 SEM images of *E. faecalis* (colored in pink in the image manipulation software Photoshop CS6) on different PMMA surfaces after different periods of incubation (scale bar = 1 μm, magnification: ×10 000).

appearance was observed after 3 days or 1 week in the control group. In contrast, there were some tiny clusters of bacteria dispersed in between the nanoprotrusions; some other cells were situated on top of the spinules. The outline of individual bacterial cells was not clear. At 72 hours and 1 week after incubation, a biofilm-like structure was frequently seen on the nanopatterned groups. All of them seemed to have been disturbed/disrupted to an extent that no individual cells could be identified. The pointed tips of the nanospinules were seen to have "pierced" through the film-like structures, especially in the NP800 and NP1200 groups. Some bacterial cells appeared stuck between the nanoprotrusions.

3.2.3 ***Porphyromonas gingivalis*.** Similar trends were observed for the samples cultured with *P. gingivalis* (Fig. 7). CLSM examination revealed remarkable differences in the bacterial growth between the smooth control and the nanopatterned surfaces (Fig. 7a). The differences between the experimental groups were relatively small. Generally, for the experimental groups, the proportion of living bacteria kept decreasing from around 85% to about 35% (NP800) to 50% (NP400 and NP1200), whereas that of the control group remained quite stable at just below 100% throughout the incubation

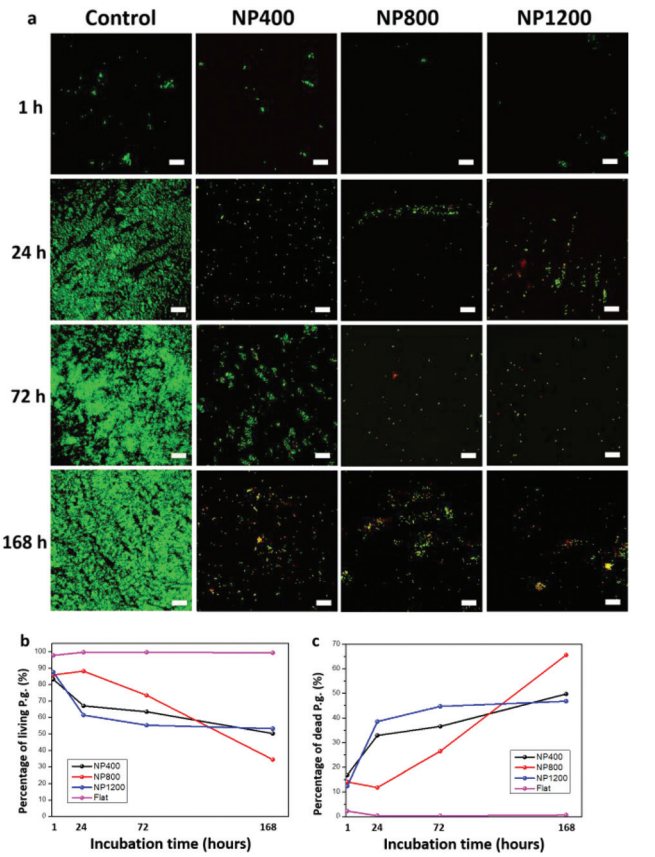

Fig. 7 Viability of *P. gingivalis* on different surfaces at different incubation times: (a) CLSM images of live (green) and dead (red) bacterial cells; (b) percentage of live *P. gingivalis*; and (c) percentage of dead *P. gingivalis* (measurement area = 126 × 126 μm^2 and image size = 640 × 640 pixels) (error bars = 95% CI, *p < 0.05).

Published on 05 August 2020. Downloaded on 4/22/2021 7:05:35 AM.

period (Fig. 7a and ESI Fig. 3†). The proportion of dead bacteria went up dramatically for the experimental groups, whereas the figure was just above 0% for the control throughout (Fig. 7b). The overall amounts of bacteria residing on the nanopatterned surfaces were significantly lower than that of the smooth control surface ($p < 0.05$).

For this slow-growing species, generally there were fewer *P. gingivalis* cells residing on the smooth surface of the control group; their number increased over time and formed thin aggregates. There were plenty of cell-to-cell contacts, but the outline of individual cells remained identifiable (Fig. 8). For the nanopatterned PMMA surfaces, at 1 hour, few bacterial cells were seen among the nanoscale protrusions. After 1 day of incubation, more cells were present in a very disordered manner, some of which were mounting on the tips, but the majority of them were lodged in the spaces in between the nanospinules. The appearance was similar at 3 days post-incubation, with the bacterial cells situated mostly in between the spinules and with little sign of biofilm formation. After 1 week, some areas with a biofilm-like structure were observed, but no identifiable cell outline could be noticed. The film-like structures appeared to have been punctured by the nanoprotrusions, especially in the NP800 and NP1200 groups. Evidence of disrupted bacterial accumulation could be observed.

3.2.4 ***Fusobacterium nucleatum.*** CLSM examination revealed a similar trend of the amount of *F. nucleatum* as with other bacterial species tested. The amount was significantly reduced on the nanopatterned surfaces at all incubation periods ($p < 0.05$). However, the difference in the number of live bacteria between the experimental groups was not statistically significant (Fig. 9 and ESI Fig. 4†).

SEM examination revealed that the packing of these filamentous bacteria was obviously less dense on the nanopatterned surfaces, compared with the smooth control (Fig. 10).

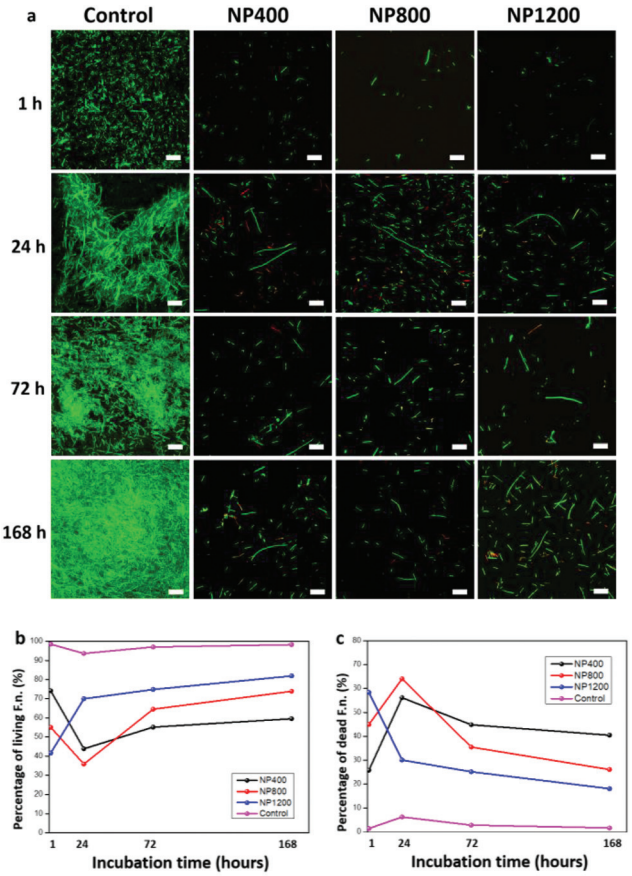

Fig. 9 Viability of *F. nucleatum* on different surfaces at different incubation times: (a) CLSM images of live (green) and dead (red) *F. nucleatum*; (b) percentage of live *F. nucleatum*; and (c) percentage of dead *F. nucleatum* (measurement area = 126 × 126 μm^2 and image size = 640 × 640 pixels) (error bars = 95% CI, *$p < 0.05$).

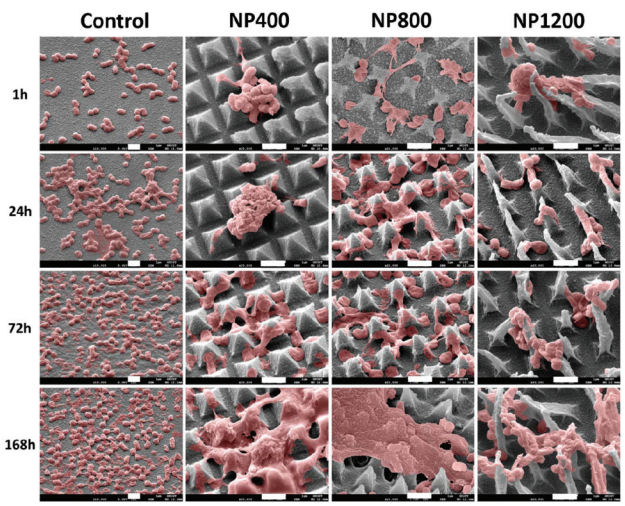

Fig. 8 SEM images of *P. gingivalis* (colored in pink in the image manipulation software Photoshop CS6) on different PMMA surfaces after different periods of incubation (scale bar = 1 μm, magnification: ×10 000).

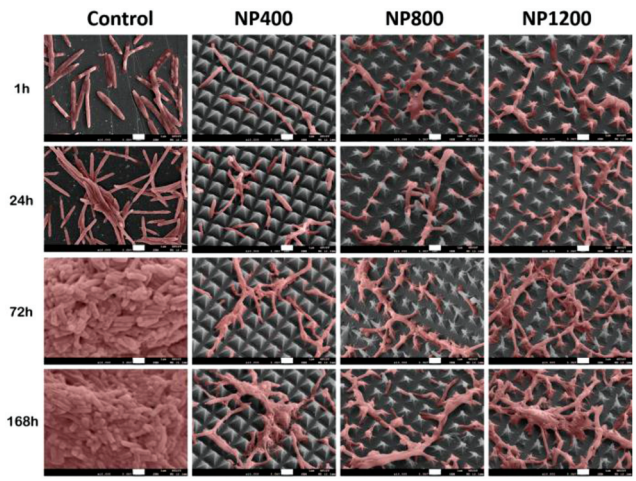

Fig. 10 SEM images of *F. nucleatum* (colored in pink in the image manipulation software Photoshop CS6) on different PMMA surfaces from 1 hour to 1 week (scale bar = 1 μm, magnification: ×10 000).

This journal is © The Royal Society of Chemistry 2020

Published on 05 August 2020. Downloaded on 4/22/2021 7:05:35 AM.

While the bacterial mass became denser and thicker on the smooth surface with time, large areas of the uncolonized region were observed for the experimental groups. During the incubation period from 1 day to 1 week, some bacterial cells that were present at the tips of the nanospinules seemed to have been ruptured, with the cell outline becoming shrunken, irregular and poorly defined, when compared with those in the control group (Fig. 10). Some filamentous cells were lodged in the valleys in between the nanoprotrusions with part of the cell outlines seemingly stretched and some parts shrunken.

One of the primary hypotheses is that the high aspect ratio surface protuberances minimise the contact area adhesion capacity of cells conforming to the surface. This phenomenon leads to the stretching and compression of the cells after they have attached to the surfaces available to them. Physical confinement and restriction on the bacteria imposed by the protuberances reduced the available surface area and capacity to form focal attachments through fimbriae, for example. In Fig. 11 the contact area occupied by living bacteria after making their first contact, in the first hour of interaction with different surface structures is quantified (ESI Fig. 5–7†). The smooth surface does not impede the bacterial attachment and chain growth, in stark contrast to surfaces 400, 800, and 1200. Among these high aspect structures the area occupied by live cells is phenomenally small. Although, the apparent differences between the pyramids with increasing aspect ratio are small (except for the *S. mutans* bacteria), the spread of dead cells is quite significant, varying between 0, 6, and 18 μm^2.

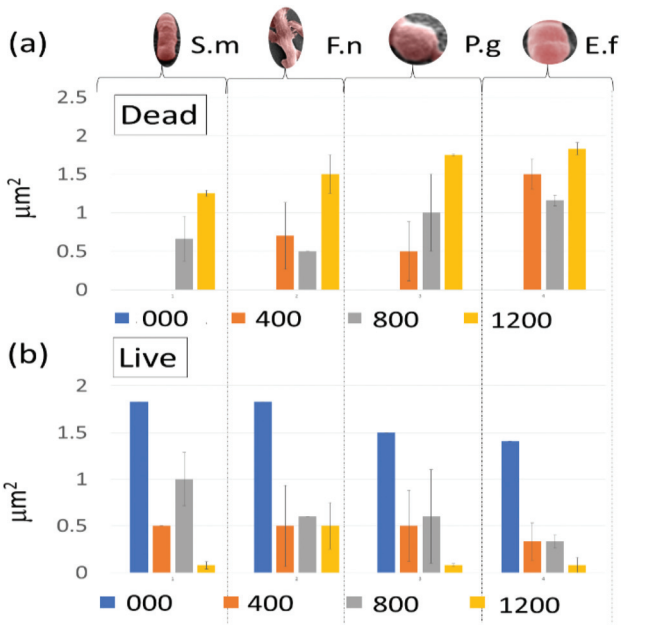

Fig. 11 The approximate area (μm^2) occupied by (a) dead bacterial cells and (b) live cells upon contact with the structured PMMA surfaces, 000 – smooth, 400, 800 and 1200. A clear and wide difference is observed between smooth and high aspect ratio nanopyramid arrays.

4. Discussion

Photolithography is a fabrication process that can produce precise surface nanostructures at a very high resolution. It is versatile and requires very little post-fabrication sample preparations.[29] Various patterns of different aspect ratios are possible using this fabrication method. By controlling the amount of chromium deposition, it is possible to control the aspect ratio of the nanoscale protrusions, for the optimization of the parameters to achieve the best result with respect to bacterial attachment and settlement. There were some variations in the measured height of the NP800 and NP1200 spinules, possibly due to stretching and deformation during peeling from the mold. These "long" spinules of the NP1200 group appear somewhat flexible, but they did not seem to affect the bactericidal properties of that surface. Mathematically, the nanoscale protrusions with a higher density or aspect ratio could lead to a greater stretching of the cell membrane and hence rupturing of the bacterial cell, as a result of an increase in the contact area.[30]

Bacterial attachment and biofilm formation are sophisticated processes. The physical interaction between the bacterial cells and surface topography is an intricate process. Not only are the size and shape of the bacterial cell, its membrane rigidity and the presence of membrane features involved in mobility, sensing, and anchorage to a surface,[32] but also the ability of bacteria to form cell–cell connections would affect their response to any topographical features.[19] Thus, a difference in behavior should be expected among different species.[19] For this reason, our *in vitro* study tested the various nanopatterned surfaces using several representative and pathogenic species of the oral microflora. It has been reported that the number of bacterial cells (*S. aureus*, *P. aeruginosa*, and *E. coli*) and of extracellular polysaccharide (EPS) attaching to a titanium surface was inversely related to the average roughness (R_a) value.[16,33] A similar result was reported for glass, such that a smooth glass surface with a R_a value of 1.3 nm mediated more attachment of eight different bacterial species than a glass surface of R_a = 2.1 nm.[34] The R_a values of the nanopatterned surfaces increased with the aspect ratio of the nano-pyramids, a phenomenon that is expected. The present results suggested that PMMA with nanoscale pyramidal projections possesses both antibiofouling and bactericidal effects against the four species of oral bacteria tested. Subjectively, the longer spinules (*i.e.* NP800 and NP1200 groups) were more often seen to penetrate through the biofilm-like structure, whereas the bacterial cells were frequently seen to be trapped among the nanoprotrusions with a lower aspect ratio as in the NP400 group. Further study of the optimal R_a, or aspect ratio, for the nanoprotrusions is warranted.

Bacteria and cells are keen to adapt to non-native environments, with an attempt to spread over and adhere to the surface. When the bacterial cells encounter an array of nanopillar nanostructures, their cell wall would be in contact with multiple pillars, leading to distortions of the cell wall at the interface and the resultant stresses would lead to the rupture

Published on 05 August 2020. Downloaded on 4/22/2021 7:05:35 AM.

of the cell.[35,36] Bacteria that actively bind to a surface might be more susceptible to such a mechanism of death by physical damage.[30] The free surface energy and spacing between the nanopillars have been suggested as important factors that favor the stretching of the bacterial wall, leading to ultimate cell death. A higher mortality rate of bacteria was proposed for the narrower spacing for the nanoscale protrusions.[30] Although a fixed spacing (of 500 nm) between the nanospinules was employed in the making of the nanopatterned surface in this study, the influence of this spacing would benefit from further experimentation to optimize this particular parameter against the pathogenic microorganisms in the mouth.

We propose a series of mechanisms for the rupturing of bacteria by the pyramid tips – pictured in Fig. 12. In brief, the bacterial cells make multiple physical contacts with the sides of the nanoprotrusions. *F. nucleatum* extends fimbrae to facilitate the attachment to the complex topography. Protrusion spacings that are slightly larger than the cells, but at distances sufficient to allow contacts with the pyramid edge, caused the bacteria to stretch themselves, to compress, and to have their cell wall punctured. We can see snapshots of the physical damage in the SEM images of the bacteria covered surfaces. The larger (10 microns) bacterial cells by length (*F. nucleatum*) are therefore 20× larger than the spacing of 0.5 μm, ruptured in SEM and killed as a result of penetration from the pyramid apices (Fig. 12). Although, a fraction of *F. nucleatum* cells aligned themselves between the pyramidal apices because the bacterial width (0.4–0.7 μm) fits between the pyramids. In this case, they are liable to rupture by overstretching as they attempt to make enough contacts for stable support and attachment. For the smaller cells than *F. nucleatum* (10 μm), including *P. gingivalis* (0.3–0.5 μm), *S. mutans*, and *E. faecalis* (0.5–1 μm), they descended between the nanopyramids. By this logic, if the spacing of the arrays decreased, the smaller cells are more easily punctured and die. This simple mechanistic model for the death of bacterial cells upon contact with differently spaced pyramids correlates with the CLSM and SEM snapshots of bacteria on the various pyramid arrangements.

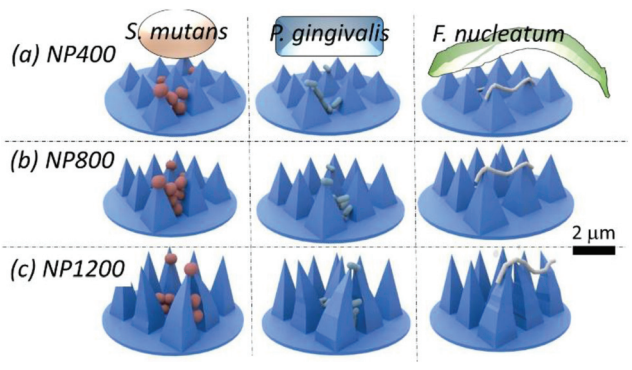

Fig. 12 Hypothesised mechanisms for bacterial cell death by tearing, rupture, and puncturing. The nano-patterned pyramidal protrusions cause the damage. Bacteria are set-up to interact with the nanoscale structures of different heights, widths, and aspect ratios: categorized into three test groups (a) NP400, (b) NP800, and (c) NP1200.

We fabricated PMMA materials with antibacterial textures against a broad range of dental pathogens. PMMA is a biomaterial with high utility in ophthalmology, dentistry, and orthopedics and as a general material used for preventing microbial contamination and disease transmission in hospital environments. Specifically, the data on oral pathogens highlight the utility of making removable partial and complete dentures. Prostheses of these kinds are often provided to the elderly or compromised individuals who may have less-than-optimal oral hygiene, the accumulation of years of wear and tear. Further study will characterize the responses of more types of bacteria, pathogens and benign species differing in size, morphology, mobility, and aggregation. In doing so, we broaden the functional reach of the pyramid motif, which can be readily inscribed in all selected materials, ceramics and particularly polymers.

Finally, we should not overlook the progress being made in harnessing metals with different surface textures for antibacterial effects against plaque formation on dental biomaterials, inside the oral cavity. Although, the reported evidence covering surface texturing is contradictory. Titanium and graphene metals offer excellent mechanical properties far exceeding those normally exhibited by several polymers and ceramic materials. Titanium is also a choice material for tooth implants for the long track record of predictable osseointegration. It is also biocompatible with gum tissue, except when colonized by a bacterial biofilm. Graphene coatings generated high levels of hydrophobicity plus lowered SFE, and consequently inhibited biofilm formation from common oral bacteria.[37,38] In addition, titanium without appreciable roughness and no protuberances either can prevent plaque formation. So, hydrophobicity can be exploited on surfaces by tuning roughness. Clearly, the high aspect ratio surface nanotopography (not termed under the umbrella of roughness), not only generates high hydrophobic forces at the boundary layer, but also gives rise to very strong physical effects on the bacteria. The physicality is the main consideration when assessing the antibiofilm capacity of high-aspect protuberance-covered surfaces. The added advantage of such surfaces is the better adhesion to tissue than that of smooth surfaces giving them higher applicability in gum-, mucosal-, periodontal- and bone-contacting oral tissues.

5. Conclusions

Nano-patterned surfaces serialized with varying dimensions of nanoscale protrusions were fabricated into the surface of PMMA and evaluated for their effectiveness against several oral pathogens to illustrate the application for a particular medical niche; and they could well adapt to other ophthalmological, endothelial niches. These selected pathogens are comprised of bacterial species with multivariate shapes (three shapes: cocci/rod and fusiform rods of spindles), three sizes (0.5–0.75 μm/

 This journal is © The Royal Society of Chemistry 2020

0.5–1.2 μm/0.4–10 μm), three capsule structures (Gram negative and Gram positive), and architectural design. In all three examples, the nanopatterned PMMA surfaces showed high levels of damage against contacting bacteria leading to mortality rates of up to 80%. Materials textured with gecko-inspired protrusions possess great utility on the film surface for medical implants and medical devices.

Conflicts of interest

There are no conflicts to declare.

Acknowledgements

This work was supported by the Hong Kong Innovation and Technology Fund (ITS/415/16) of the Innovation and Technology Commission of Hong Kong SAR, the Endodontic Research Fund of the University of Hong Kong Faculty of Dentistry (Account No.: 102009653.012058.08008.310), the National Natural Science Foundation of China (Project No. 51672231 and 81901058), the Shenzhen Science and Technology Innovation Commission (Project No. JCYJ20170818114107730), the Natural Science Foundation of Shenzhen University General Hospital (SUGH2020QD007), and the Shenzhen Key Medical Discipline Construction Fund. The authors also wish to express their gratitude to the Nanosystem Fabrication Facility (NFF) of HKUST for helping with nanofabrication.

Published on 05 August 2020. Downloaded on 4/22/2021 7:05:35 AM.

Notes and references

1 B. Schachter, *Nat. Biotechnol.*, 2003, **21**, 361.
2 A. F. Han, J. K. H. Tsoi, F. P. Rodrigues, J. G. Leprince and W. M. Palin, *Int. J. Adhes. Adhes.*, 2016, **69**, 58.
3 M. A. Curtis, C. Zenobia and R. P. Darveau, *Cell Host Microbe*, 2011, **10**, 302.
4 M. Oilo and V. Bakken, Biofilm and Dental Biomaterials, *Materials*, 2015, **8**(6), 2887–2900.
5 P. J. M. Bispo, W. Haas and M. S. Gilmore, *Pathogens*, 2015, **4**, 111.
6 M. Katsikogianni and Y. F. Missirlis, *Eur. Cells Mater.*, 2004, **8**, 37.
7 R. Q. Frazer, R. T. Byron, P. B. Osborne and K. P. West, *J. Long-Term Eff. Med. Implants*, 2005, **15**, 629.
8 C. Sahin, A. Ergin, S. Ayyildiz, E. Cosgun and G. Uzun, *J. Adv. Prosthodontics*, 2013, **5**, 140.
9 F. E. Dewhirst, T. Chen, J. Izard, B. J. Paster, A. C. R. Tanner, W.-H. Yu, A. Lakshmanan and W. G. Wade, *J. Bacteriol.*, 2010, **192**, 5002.
10 A. K. Epstein, B. Pokroy, A. Seminara and J. Aizenberg, *Proc. Natl. Acad. Sci. U. S. A.*, 2011, **108**, 995.
11 R. J. Fair and Y. Tor, *Perspect. Med. Chem.*, 2014, **6**, 25.
12 H. van de Belt, D. Neut, W. Schenk, J. R. van Horn, H. C. van der Mei and H. J. Busscher, *Acta Orthop. Scand.*, 2001, **72**, 557.
13 D. McShan, P. C. Ray and H. Yu, *J. Food Drug Anal.*, 2014, **22**, 116.
14 M. R. Anaraki, A. Jangjoo, F. Alimoradi, S. M. Dizaj and L. Farzaneh, *Pharm. Sci.*, 2017, **23**, 207.
15 C. M. Tan, J. K. Tsoi, C. J. Seneviratne and J. P. Matinlinna, *J. Prosthodontics Res.*, 2014, **58**, 243.
16 W. Teughels, N. Van Assche, I. Sliepen and M. Quirynen, *Clin. Oral Implants Res.*, 2006, **17**, 68.
17 G. P. Feng, Y. F. Cheng, S. Wang, D. A. Borca-Tasciuc, R. W. Worobo and C. I. Moraru, *npj Biofilms Microbiomes*, 2015, **1**, 9.
18 K. Anselme, P. Davidson, A. M. Popa, M. Giazzon, M. Liley and L. Ploux, *Acta Biomater.*, 2010, **6**, 3824.
19 D. Perera-Costa, J. M. Bruque, M. L. Gonzalez-Martin, A. C. Gomez-Garcia and V. Vadillo-Rodriguez, *Langmuir*, 2014, **30**, 4633.
20 S. M. Kelleher, O. Habimana, J. Lawler, B. O' Reilly, S. Daniels, E. Casey and A. Cowley, *ACS Appl. Mater. Interfaces*, 2016, **8**, 14966.
21 E. P. Ivanova, J. Hasan, H. K. Webb, V. K. Truong, G. S. Watson, J. A. Watson, V. A. Baulin, S. Pogodin, J. Y. Wang, M. J. Tobin, C. Lobbe and R. J. Crawford, *Small*, 2012, **8**, 2489.
22 J. Hasan, H. K. Webb, V. K. Truong, S. Pogodin, V. A. Baulin, G. S. Watson, J. A. Watson, R. J. Crawford and E. P. Ivanova, *Appl. Microbiol. Biotechnol.*, 2013, **97**, 9257.
23 X. Li, *Phys. Chem. Chem. Phys.*, 2016, **18**, 1311.
24 G. S. Watson, D. W. Green, M. Sun, A. Liang, X. Li, B. W. Cribb and J. A. Watson, *J. Nanosci. Adv. Technol.*, 2015, **1**, 1.
25 C. W. Kaplan, R. Lux, S. K. Haake and W. Shi, *Mol. Microbiol.*, 2009, **71**, 35.
26 WHO fact sheet, https://www.who.int/news-room/fact-sheets/detail/oral-health (accessed 22 July 2020).
27 G. S. Watson, D. W. Green, L. Schwarzkopf, X. Li, B. W. Cribb, S. Myhra and J. A. Watson, *Acta Biomater.*, 2015, **21**, 119.
28 X. Li, G. S. P. Cheung, G. W. Watson, J. A. Watson, S. Lin, L. Schwarzkopf and D. W. Green, *Nanoscale*, 2016, **8**, 18860.
29 K. H. Tsui, X. Li, J. K. H. Tsoi, S. F. Leung, L. Tang, W. Y. Chak, C. Zhang, J. Chen, G. S. P. Cheung and Z. Fan, *Nanoscale*, 2018, **10**, 10436.
30 G. A. Watson, D. W. Green, J. Watson, Z. Zhou, X. Li, G. S. P. Cheung and M. Gellender, *Adv. Mater. Interfaces*, 2019, **6**, 1801646.
31 D. Sun and K. F. Böhringer, *Micromachines*, 2019, **10**, 101.
32 G. P. Feng, Y. F. Cheng and S. Wang, *npj Biofilms Microbiomes*, 2015, **1**, 9.
33 A. Han, J. K. H. Tsoi, J. P. Matinlinna, Y. Zhang and Z. Chen, *Dent. Mater.*, 2018, **34**, 272.
34 M. Quirynen, H. C. van der Mei, C. M. Bollen, A. Schotte, M. Marechal, G. I. Doornbusch, I. Naert, H. J. Busscher and D. van Steenberghe, *J. Dent. Res.*, 1993, **72**, 1304.
35 R. D. Turner, A. F. Hurd, A. Cadby, J. K. Hobbs and S. J. Foster, *Nat. Commun.*, 2013, **4**, 1496.

36 B. A. Aguado, W. Mulyasasmita, J. Su, K. J. Lampe and S. C. Heilshorn, *Tissue Eng.*, 2012, **18**, 806.
37 R. Bürgers, T. Gerlach, S. Hahnel, F. Schwarz, G. Handel and M. Gosau, *Clin. Oral Implants Res.*, 2010, **21**, 156.
38 S. V. Agarwalla, K. Ellepola, M. C. F. Costa, G. J. M. Fechine, J. L. P. Morin, A. H. C. Neto, C. J. Seneviratne and V. Rosa, *Dent. Mater.*, 2019, **35**, 403.

Published on 05 August 2020. Downloaded on 4/22/2021 7:05:35 AM.

This journal is © The Royal Society of Chemistry 2020